Proceedings of the International Conference "Condensed Matter Physics", Jaszowiec 2000

ELECTRONIC AND TRANSPORT PROPERTIES OF RAgSn (R=Ce, Pr, Nd, Dy) COMPOUNDS

D. Fus[a], V. Ivanov[b], A. Jezierski[c], B. Penc[a] and A. Szytuła[a,*]

[a]Institute of Physics, Jagiellonian University, Reymonta 4, 30-059 Kraków, Poland
[b]General Physics Institute, Academy of Sciences, 117742 Moscow, Russia
[c]Institute of Molecular Physics, Polish Academy of Sciences
Smoluchowskiego 17, 60-179 Poznań, Poland

The electronic structure of the ternary RAgSn (R=Ce,Pr,Nd,Dy) compounds which crystallize in the hexagonal LiGaGe-type structure was studied by X-ray photoemission spectroscopy. Core-levels and valence bands were investigated. The X-ray photoemission spectroscopy valence bands are compared with the ones calculated using the spin-polarized tight-binding linear muffin-tin orbital method. The obtained results indicate that the valence bands are mainly determined by the Ag $4d$ band. The spin–orbit splitting values Δ_{SO} determined from the XPS spectra of $3d_{5/2}$ and $3d_{3/2}$ are equal to 18.8 eV for R = Ce, 20.2 eV for R = Pr and 22.6 eV for R = Nd. The analysis of these spectra on the basis of the Gunnarsson–Schönhammer model gives a hybridization of f orbitals with the conduction band. The calculation of the total energy for two models of the crystal structure: an ordered of the LiGaGe-type and a disordered one of the $CaIn_2$-type indicate that in these compounds the LiGaGe-type structure is stable. Additionally, the temperature dependences of the electrical resistivity of CeAgSn and DyAgSn are investigated. At high temperatures the resistivity is not a linear function of temperature which indicates an electron–phonon interaction in the presence of a small s–d scattering, whereas at low temperatures anomalies connected with the magnetic phase transitions are observed.

PACS numbers: 71.20.–b, 72.15.Eb, 79.60.–i

1. Introduction

The RTSn ternary intermetallic compounds (R — rare earth, T — transition metals) form a large family of systems with different crystallographic structures and different physical properties. In these compounds the rare earth moments form a variety of magnetic structures at low temperatures [1]. The RAgSn compounds, except for EuAgSn, were found by X-ray diffraction to crystallize in the

*corresponding author; e-mail: szytula@if.uj.edu.pl

hexagonal $CaIn_2$-type structure [2] but new neutron diffraction data show that these compounds have the hexagonal LiGaGe-type structure in which Ag and Sn atoms are in two sublattices [3]. Magnetic susceptibility and electric conductivity measurements [4, 5], supplemented by neutron diffraction studies, show that these compounds exhibit an antiferromagnetic ordering at low temperatures [3, 6, 7].

This paper reports on the results of X-ray photoemission spectroscopy (XPS) measurements for RAgSn (R = Ce,Pr,Nd,Dy) compounds. The XPS valence band spectra are compared with *ab-initio* electronic structure calculations using the tight-binding linear muffin-tin orbital (TB LMTO) method [8]. For CeAgSn and DyAgSn the additional electric resistivity vs. temperature measurements are performed. On the basis of these results the electronic structure of the compounds have been determined.

2. Experimental

All experiments were performed on as-sintered pellets in a vacuum of about 10^{-9} mbar.

The XPS spectra were obtained at room temperature using the Leybold LHS10 electron photoemission spectrometer with Mg K_α ($h\nu = 1253.6$ eV) radiation. The total energy resolution of the spectrometer with a hemispherical energy analyser was about 0.75 eV for Ag $3d$. Binding energies are referred to the Fermi level ($E_F = 0$). The spectrometer was calibrated using the Cu $2p_{3/2}$ (932.5 eV), Ag $3d_{5/2}$ (368.1 eV) and Au $4f_{7/2}$ (84.0 eV) core-level photoemission spectra. Measurements were carried out at room temperature. Surfaces of the compounds were mechanically cleaned by scraping with a diamond file in a preparation chamber under high vacuum (10^{-9} mbar) and then, immediately moved into the analysis chamber. This procedure was repeated until the C $1s$ and O $1s$ core-level peaks were negligibly small or did not change after further scrapings. Such a procedure of cleaning was performed before each XPS measurement. The Shirley method [9] was used to subtract the background and so prepared experimental spectra were numerically fitted using the 80% Gaussian and 20% Lorentzian model.

The electrical resistivity measurements were taken in the temperature interval of 2–300 K using a conventional four-point-probe method.

3. The method of calculation

The electronic structure was calculated by *ab-initio* self-consistent TB LMTO method [8] within the framework of the local spin density (LSD) approximation. The scalar-relativistic approximation for band electrons and the fully-relativistic treatment of the frozen core electrons were used. The exchange correlation potential was assumed in the form of von Barth and Hedin [10] with gradient corrections [11]. The self-consistent calculations were performed in the atomic sphere approximation (ASA) for the experimental values of the lattice parameters. The values of the atomic sphere radii were chosen in such a way that the sum of all

atomic sphere volumes was equal to the volume of the unit cell. In the band calculations the initial atomic configurations were assumed according to the periodic table of elements.

The magnetic moment was calculated by spin-polarized TB LMTO method. The scheme proposed by Brooks et al. [12] in which the $4f$ states of rare earth atoms are treated as open core states was applied. In this model the $4f$ states of rare earth (RE) did not hybridize with the conduction electron states and the number of $4f$ electrons of RE was fixed to be integer. The spin-polarized band calculations for the full hybridization of s, p, d, and f electrons were also performed and the results are presented in Sec. 5. The theoretical photoemission spectra were obtained from the calculated density of states (DOS) convoluted by a Lorentzian with a half-width equal to 0.4 eV and scaled using the proper photoelectric cross sections for partial states [13].

4. Results of the XPS measurements

Figure 1 shows the XPS spectra of the RAgSn (R = Ce,Pr,Nd, and Dy) compounds in a wide binding energy range of 0–1100 eV. Binding energies are related to the Fermi level (E_F = 0 eV). A small contamination of oxygen and carbon is visible.

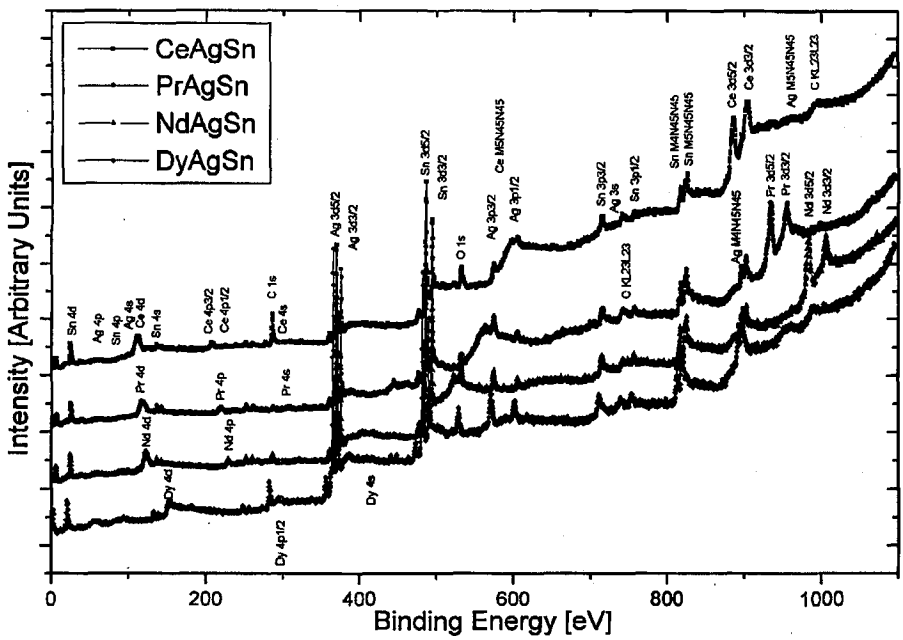

Fig. 1. XPS Mg K_α spectra of the RAgSn (R = Ce,Pr,Nd,Dy) compounds (with the core level lines) in the wide binding energy range of 0–1100 eV.

4.1. XPS valence bands

The XPS valence bands (VB) of all the investigated compounds are presented in Fig. 2. The bands extend from the Fermi energy, located at $E = 0$, to the binding energy of about 15 eV. The XPS spectrum of CeAgSn represents mainly a dominant contribution of Ag $4d$ states. A broad and very weak peak about 1 eV corresponds to the Ce $4f$ and $(5d6s)^3$ states [14]. In the XPS valence bands of PrAgSn and NdAgSn the broad peaks corresponding to the Ag $4d_{3/2}$ and $4d_{5/2}$ states are also dominant. The small intensity peaks about 1.0, 3.3, and 8.1 eV in the spectra of both compounds correspond to the $(5d6s)^3$ states, Sn $5p$ or/and $4f$ rare earth and Sn $5s$, respectively.

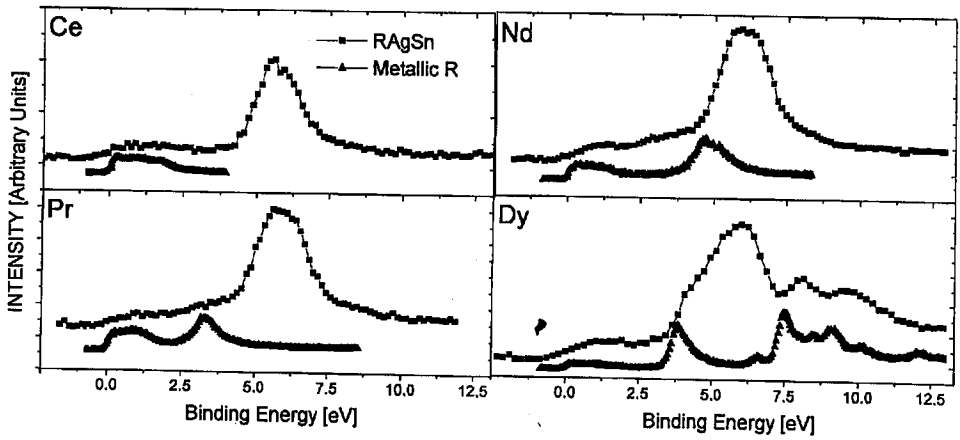

Fig. 2. XPS spectra of valence bands in the RAgSn (R = Ce,Pr,Nd,Dy) compounds and the appropriate spectra for metallic Ce,Pr,Nd, and Dy (after [15]).

The spectrum of DyAgSn consists not only of the Ag $4d$ but also of Dy $4f$ bands.

4.2. Core levels

Peaks corresponding to the $5p_{1/2}$, $5p_{3/2}$, $4d_{3/2}$, $4d_{5/2}$, $3d_{3/2}$, and $3d_{5/2}$ states of rare earth elements to the $3d_{3/2}$, $3d_{5/2}$, $3p_{1/2}$, $3p_{3/2}$ of Ag, as vell as to the $4d_{3/2}$, $4d_{5/2}$, $3d_{3/2}$, $3d_{5/2}$, $3p_{1/2}$, and $3p_{3/2}$ of Sn are clearly visible (Fig. 1). Table I collects the determined values of the energy levels and values of ΔE for some levels of the RAgSn (R = Ce,Pr,Nd,Dy) compounds. The obtained results indicate that the values of energy levels does not change with the change of the $4f$ element and is in good agreement with the values in Ref. [15].

In the case of CeAgSn the characteristic multiplet structure is due to the $4d^9 4f^1$ states with the energy levels equal to 109.3 eV for Ce $4d_{5/2}$ and 111.4 eV for Ce $4d_{3/2}$ and ΔE equal to 2.1 eV. For PrAgSn and NdAgSn broad peaks with the energy 115.9 eV and 121.3 eV, respectively, are observed. These values are in good agreement with the values in Ref. [16].

TABLE I

Values of the energy levels (in [eV]) of $3d_{5/2}$ and $3d_{3/2}$ of Ag; $4d_{5/2}$, $4d_{3/2}$, $4s$, $3d_{5/2}$, and $3d_{3/2}$ of Sn and respective values of ΔE (in [eV]) for the RAgSn (R = Ce,Pr,Nd, and Dy) series of compounds. For comparison the appropriate values of pure Ag and Sn are also listed.

Compound	Energy								
	Ag			Sn					
	$3d_{5/2}$	$3d_{3/2}$	ΔE	$4d_{5/2}$	$4d_{3/2}$	ΔE	$3d_{5/2}$	$3d_{3/2}$	ΔE
CeAgSn	368.3	374.3	6.0	23.0	24.0	1.0	484.7	493.2	8.5
PrAgSn	368.8	374.8	6.0	23.6	24.6	1.0	484.7	493.2	8.5
NdAgSn	368.9	374.9	6.0	23.7	24.8	1.1	485.0	493.4	8.4
DyAgSn	368.4	374.4	6.0	23.7	24.8	1.1	484.7	493.1	8.6
pure element	368.1	374.0	5.9	23.8	24.8	1.0	484.9	493.1	8.2

The Dy $4d$ core-level photoemission spectrum of DyAgSn is presented in Fig. 3. The multiplet structure of Dy $4d$ state is visible. The positions of the peaks are in good agreement with the ones calculated previously for metallic Dy in Ref. [17].

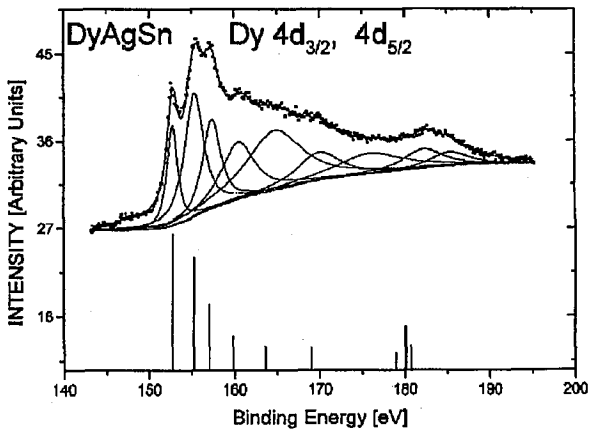

Fig. 3. Dy $4d$ core level photoemission spectrum of DyAgSn; the strokes indicate the position of the peaks corresponding to the multiplet structure (according to [17]).

Figure 4 illustrates the Ce, Pr, and Nd $3d$ XPS spectra of the investigated RAgSn (R = Ce,Pr,Nd) compounds. The structure of the $3d$ XPS spectra of RAgSn (R = Ce,Pr,Nd) has been interpreted in terms of the Gunnarsson–Schönhammer theory [18]. The spin–orbit splitting dominates the spectral structure of $3d$ XPS peaks. The $3d$ spin–orbit splitting in these compounds is equal to 18.8 eV for R = Ce, 20.2 eV for R = Pr and 22.6 eV for R = Nd. At low-binding-energy side of the $3d_{5/2}$ and $3d_{3/2}$ main lines of shake down satellites are observed which

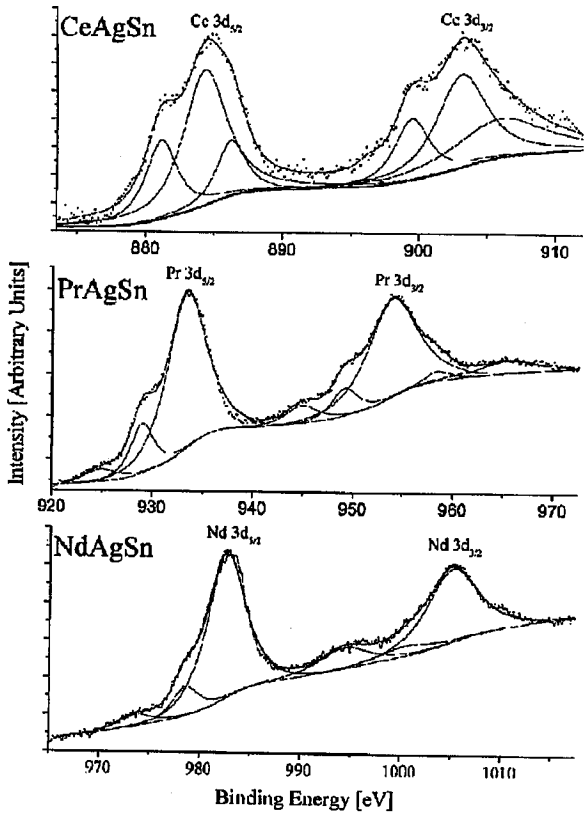

Fig. 4. X-ray photoemission spectra of $3d_{5/2}$ and $3d_{3/2}$ electron states of Ce,Pr,Nd in CeAgSn, PrAgSn, and NdAgSn.

are known to account for the screened Ce $3d^9 4f^2$, Pr $3d^9 4f^3$, and Nd $3d^9 4f^4$ final states [19]. The Ce $3d$ XPS spectrum is dominated by peaks at 884.4 eV and 903.1 eV which correspond to $3d^9_{5/2}4f^1$ and $3d^9_{3/2}4f^1$ states. The peaks at 881.4 eV and 899.0 eV are $3d^9_{5/2}4f^2$ and $3d^9_{3/2}4f^2$ satellites. The peaks at 886.5 eV and 905.9 eV come from the impurity (cerium oxides) [20].

In the PrAgSn XPS spectrum (see Fig. 4) the peaks at 929.0 eV and 949.6 eV were identified as Pr $3d_{5/2}4f^3$ and $3d_{3/2}4f^3$ satellites while those at 933.4 eV and 950.4 eV as $3d_{5/2}4f^2$ and $3d_{3/2}4f^2$ ones. The additional small peaks correspond to Pr_2O_3 impurity [21]. The small intensity peak at about 970 eV is the oxygen $1s$ Auger line [22].

A similar distribution of the peaks is observed in XPS spectrum of NdAgSn. The peaks at 982.7 eV and 1005.2 eV correspond to the $3d^9_{5/2}4f^3$ and $3d^9_{3/2}4f^3$ configuration, at 978.6 eV and 1000.5 eV correspond to satellites $3d_{5/2}4f^4$ and $3d_{3/2}4f^4$ while those at 973.6 eV and 994.4 eV correspond to the Nd_2O_3 impurity [23]. The shift of the shake down satellites, in relation to the main peak, is about 3.0 eV for Ce, 4.4 eV for Pr and 4.1 eV for Nd.

The separation of the peaks was based on the Doniach–Šunjić theory [24] which gives the intensity ratio $r = I(f^{n+1})/[I(f^n) + I(f^{n+1})]$. It was possible to determine the coupling parameter Δ using measured intensities of the final $3d^9f^1$ and $3d^9f^2$ states as well as calculations of the intensity ratio r as a function of Δ previously published. The coupling parameter Δ is defined as $\pi V^2 \rho_{\max}$, where $\rho_{\max}$ is the maximum of the density of conduction states and V is the hybridization. On the basis of the Gunnarsson–Schönhammer model a crude estimation of Δ for Pr and Nd ions seems to be possible if one assumes [25] that for Pr and Nd the calculated intensity ratio r changes with Δ the same as in the case of Ce [19].

The r value of CeAgSn equals 0.32 which corresponds to the hybridization energy 165 meV. A similar calculation for PrAgSn and NdAgSn gives r equal 0.16 and 0.12 and the adequate hybridization energies 78 meV and 62 meV. This results indicate that with an increase in the number of $4f$ electrons the hybridization energy decreases. For Ce intermetallic compounds with a strong f shell instability Δ is about 150 meV [19], while it is 160 meV for $PrNi_2X_2$ (X = Sn,Sb) [22] and 100 meV for $PdPr_{0.014}$ [25].

5. Electronic structure

The electronic structures of CeAgSn, PrAgSn, and NdAgSn were calculated in two models of crystal structure that were reported [2, 3] for these compounds. The first one is the $CaIn_2$-type of structure (proposed on the basis of X-ray data [2]). In this structure rare earth atoms occupy the 2(b) site: 0,0,1/4 and 0,0,3/4 and Ag and Sn are distributed randomly in the site $4f$: $1/3, 2/3, z$; $2/3, 1/3, 1/2 + z$; $2/3, 1/3, \overline{z}$; $1/3, 2/3, 1/2 - z$. In the LiGaGe-type of structure the atoms occupy the following positions: rare earth atoms are in 2(a): 0,0,0; 0,0,1/2; Ag atoms in 2(b): $1/3, 2/3, z_1$; $2/3, 1/3, 1/2 + z_1$ and Sn atoms in 2(b): $1/3, 2/3, z_2$; $2/3, 1/3, 1/2 + z_2$. The calculated values of the total energy for both models are collected in Table II. In all the cases the value of the total energy for the LiGaGe-type structure is smaller than for the $CaIn_2$-type. It suggests that rather the LiGaGe-type structure is stable and it is in agreement with the neutron diffraction data [3].

TABLE II

The values of the total energy (in [Ryd]) calculated for two models of the crystal structure ($CaIn_2$ and LiGaGe) for RAgSn (R = Ce, Pr, Nd, Dy) compounds.

R	$CaIn_2$	LiGaGe
Ce	−81385.5251	−81385.6319
Pr	−82892.5292	−82892.6394
Nd	−84438.7167	−84438.8294
Dy	−94568.8359	−94568.9954

The total and partial densities of states for RAgSn (R = Ce,Pr,Nd) compounds in both models of the crystal structure were calculated. The obtained results (presented in Figs. 5–8) indicate that the valence band of these compounds is displayed by a strong peak corresponding to the Ag $4d$ state at 5.5 eV and Sn $5s$ state about 7.5 eV for the LiGaGe-type structure. The data obtained for the $CaIn_2$-type structure are different. The Ag $4d$ states are represented by two peaks at 5.0 and 4.4 eV. A comparison of the calculated and observed data, presented in Table III and in Figs. 5–8, shows better agreement with the experimental results for the LiGaGe-type of crystal structure. The $4f$ level of Ce in CeAgSn, of Pr in PrAgSn and of Nd in NdAgSn is close to the Fermi level and has a very small intensity (practically not observed in XPS spectra).

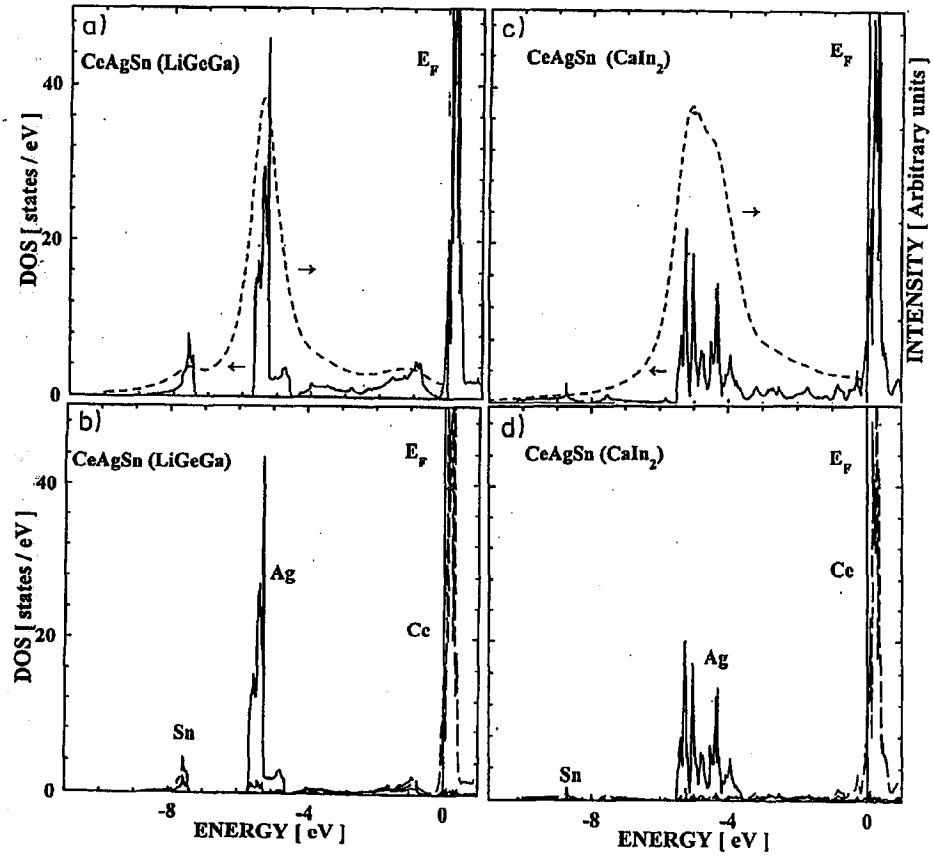

Fig. 5. The total density of states and the contribution from Ce ($6s$, $6p$, $5d$, and $4f$ electrons), Ag and Sn to the total density of states of paramagnetic CeAgSn compound for LiGaGe (a,b) and $CeIn_2$ (c,d) types of crystal structure. The Fermi level is located at $E = 0$ eV. The dashed line presents the density of states convoluted by Lorentzians of half-width 0.4 eV and multipled by the appropriate cross sections (after [13]).

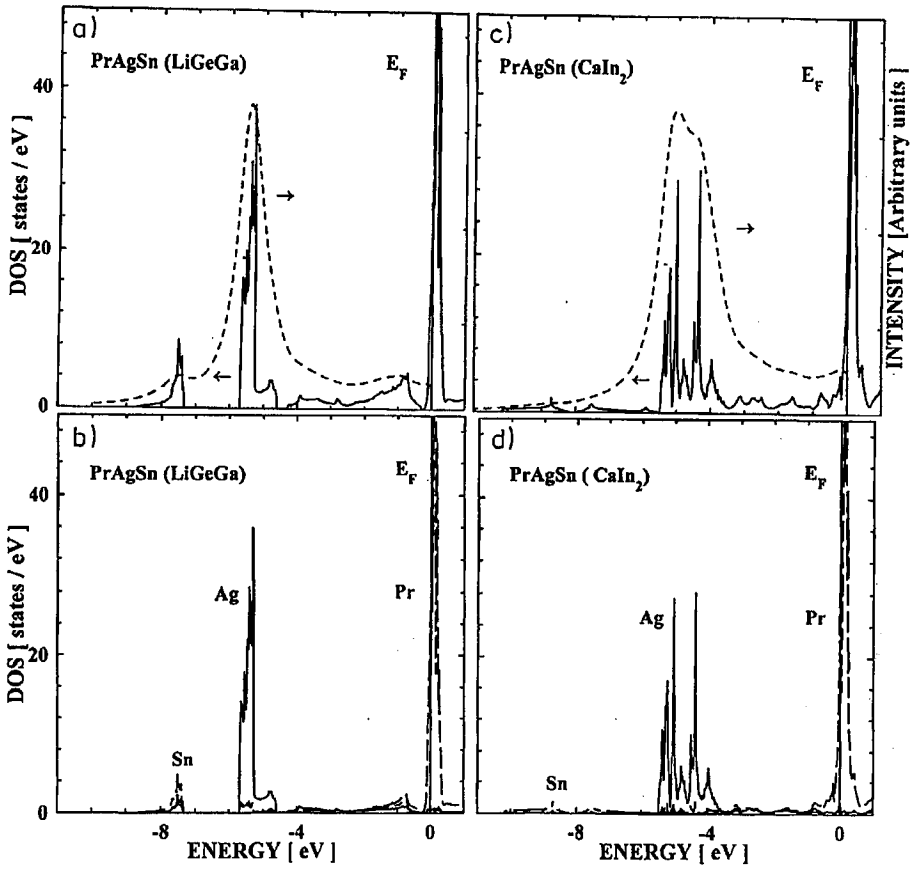

Fig. 6. The total density of states and the contribution from Pr ($6s$, $6p$, $5d$, and $4f$ electrons), Ag and Sn to the total density of states of paramagnetic PrAgSn compound for LiGaGe (a,b) and $CeIn_2$ (c,d) types of crystal structure. The Fermi level is located at $E = 0$ eV. The dashed line presents the density of states convoluted by Lorentzians of half-width 0.4 eV and multipled by the appropriate cross sections (after [13]).

The results of the electronic structure calculations, which are in good agreement with XPS spectra, show that for RAgSn (R = Ce,Pr,Nd) the density of states at the Fermi level is formed by $4f$ electrons of rare earth atoms. This matches well with self-consistent *ab initio* calculations, reported for the electronic structure of isostructural CeAuGe where the Ce $4f$ bands are found to be located at the Fermi level and 1 eV above it [26, 27].

The calculated values of the density of states $N(E_F)$ for LiGaGe-type of structure are: 11.5 [states/eV·spin f.u.] for CeAgSn, 1.35 [states/eV·spin f.u.] for PrAgSn, 13.2 [states/eV·spin f.u.] for NdAgSn and 0.3 [states/eV·spin f.u.] for DyAgSn. The $N(E_F)$ was experimentally determined, from the electronic specific heat, for CeAgSn only ($\gamma = 210$ mJ/mol·K^2) [28] and the obtained value ($N(E_F) =$ 8.9 [states/eV·spin f.u.]) is much smaller than the calculated one.

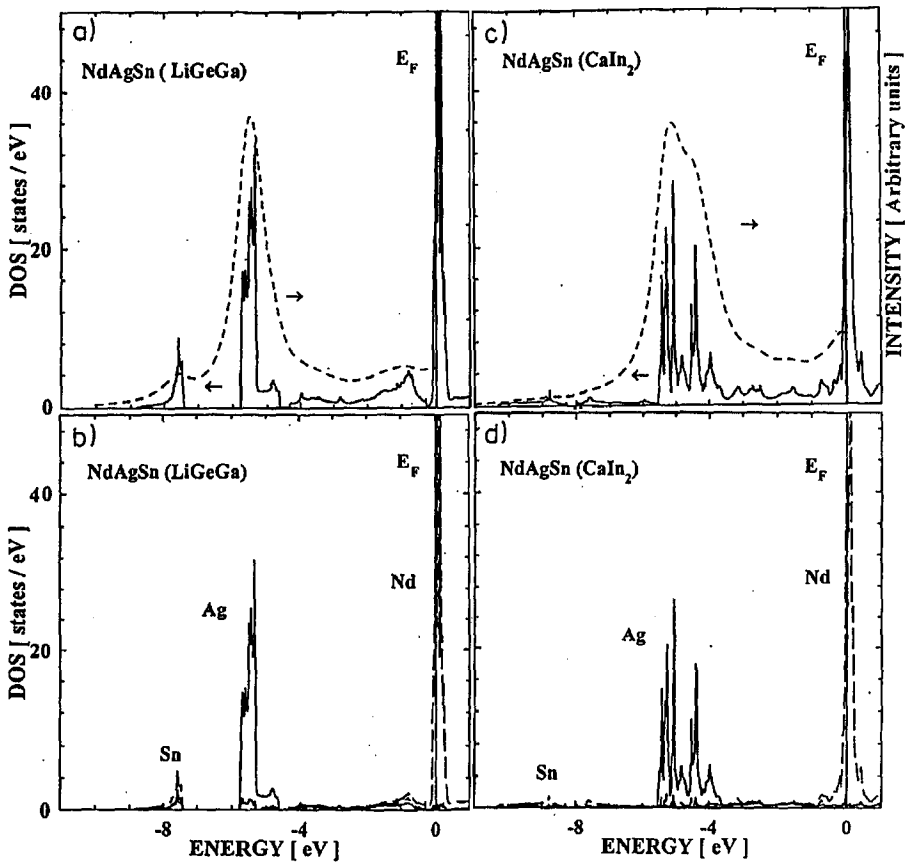

Fig. 7. The total density of states and the contribution from Nd ($6s$, $6p$, $5d$, and $4f$ electrons), Ag and Sn to the total density of states of paramagnetic NdAgSn compound for LiGaGe (a,b) and $CeIn_2$ (c,d) types of crystal structure. The Fermi level is located at $E = 0$ eV. The dashed line presents the density of states convoluted by Lorentzians of half-width 0.4 eV and multipled by the appropriate cross sections (after [13]).

As it was mentioned in Sec. 3 the magnetic moments were calculated in two different models. In the first model we have assumed a full hybridization of s, p, d, and f electrons while in the second one the Brooks model [12] was applied. The calculated values of the total magnetic moment and of the rare earth are compared with the experimental data in Table IV. A small difference between the values of the magnetic moments calculated in the Brooks model and in the *spdf* model suggests a small negative contribution from the Ag and Sn atoms to the total magnetic moment. The experimental values are smaller than the calculated ones but the ratio of the calculated as well as experimental magnetic moments to the R^{3+} ion value increases with the number of $4f$ electrons from 1 for CeAgSn to 3 for NdAgSn. It is in agreement with a decrease in hybridization in the studied compounds observed in this work.

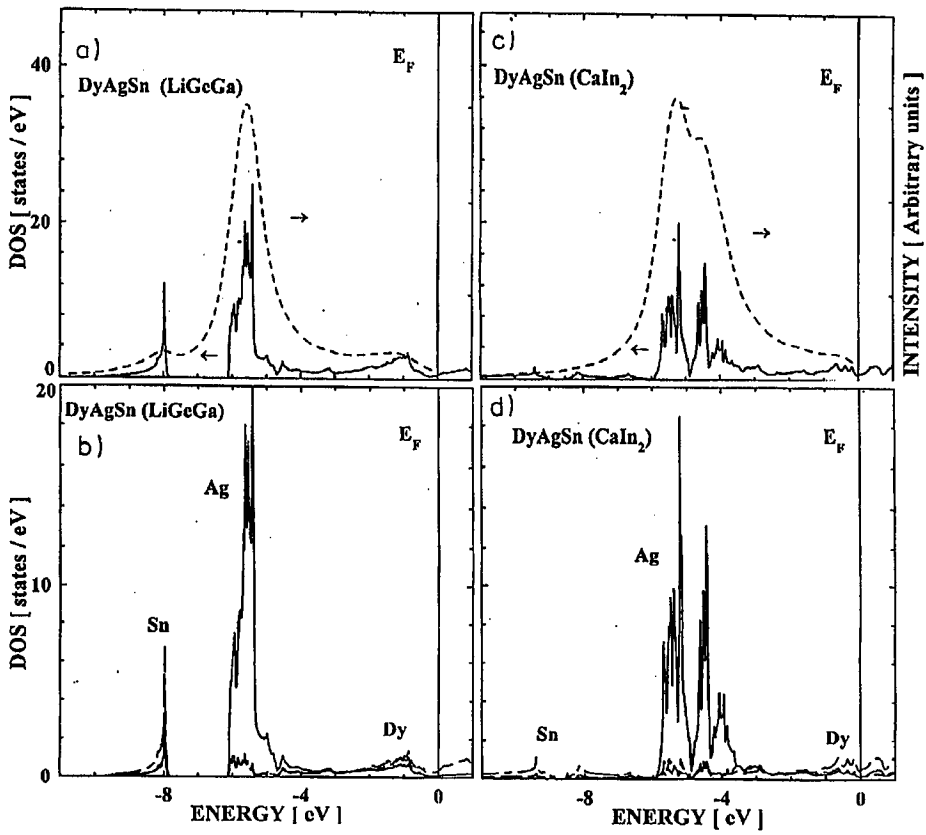

Fig. 8. The total density of states and the contribution from Dy ($6s$, $6p$, $5d$, and $4f$ electrons), Ag and Sn to the total density of states of paramagnetic DyAgSn compound for LiGaGe (a,b) and $CeIn_2$ (c,d) types of crystal structure. The Fermi level is located at $E = 0$ eV. The dashed line presents the density of states convoluted by Lorentzians of half-width 0.4 eV and multipled by the appropriate cross sections (after [13]).

TABLE III

Calculated and observed values of the energy levels for photoemission peaks of Ag $4d$ and Sn $5s$ in the RAgSn (R = Ce, Pr, Nd, Dy) compounds for two models of the crystal structure: LiGaGe and $CaIn_2$.

Compound	E(Ag $4d$) [eV]				E(Sn $5s$) [eV]		
	calc.			obs.	calc.		obs.
	LiGaGe	$CaIn_2$			LiGaGe	$CaIn_2$	
CeAgSn	5.3	5.0	4.4	5.3	7.5	8.7	8.7
PrAgSn	5.5	5.0	4.4	5.8	7.5	8.7	8.7
NdAgSn	5.5	5.1	4.4	5.9	7.5	8.8	8.8
DyAgSn	5.5	5.2	4.6	6.0	8.0	9.4	–

TABLE IV

Values of the magnetic moments of RAgSn (R = Ce,Pr,Nd,Dy) compounds μ_{tot} and of rare earth atoms μ_R only. In μ_{tot} a small contribution from Ag and Sn atoms is also included.

Compound	*spd* (Brooks model [12])		*spdf*		Experimental	Free ion
	$\mu_{tot}(\mu_B)$	$\mu_R(\mu_B)$	$\mu_{tot}(\mu_B)$	$\mu_R(\mu_B)$	$\mu(\mu_B)$	$R^{3+}(\mu_B)$
CeAgSn	1.04	1.05	1.00	1.02	0.72[a], 1.2[b]	2.14
PrAgSn	2.06	2.09	2.11	2.21	1.88[a]	3.2
NdAgSn	3.08	3.12	3.23	3.36	1.97[a]	3.27
DyAgSn	10.08	10.13			6.8[a]	10.0

[a]from neutron diffraction [3], [b]from magnetization [32]

An anomalous dependence of the Néel temperature of the compounds with R = Ce, Pr, Nd as a function of the de Gennes factor [3] is similar to that observed in the case of RGa_2 compounds [29]. It suggests a local coupling between $4f$ and conduction electrons. The coupling is much stronger than the expected one which could be due to a large orbital contribution to the exchange coupling [30].

6. Electrical resistivity measurements

Because the electrical-transport properties are very sensitive to the electronic structure the measurements of electrical resistivity of CeAgSn and DyAgSn in the function of temperature were performed. The obtained results are shown in Fig. 9. A standard analysis of the resistivity of crystalline alloys is based on the assumption that the contributions of different physical origins are additive (Matthiesens rule) [31]. Thus,

$$R(T) = R_0 + R_{ph}(T) + R_{mag}(T),$$

where R_0 is a residual resistivity due to an elastic scattering of electrons from defects and impurities and it is supposed to be independent of temperature, $R_{ph}(T)$ is a temperature-dependent term resulting from an elastic scattering of electrons from phonons, and $R_{mag}(T)$ is a term which includes other effects such as magnetic scattering.

At low temperatures, anomalies around the Néel temperature, are visible. In the inset in Fig. 9 the temperature dependence of the dR/dT is presented. In the lowest-temperature region ($T < T_N$) the magnetic properties of CeAgSn are different from those observed in DyAgSn. In the CeAgSn resistivity is a linear function of temperature, whereas for the DyAgSn it shows the T^2 behaviour. The relation for the least-squares fit can be expressed by $\varrho(T) = \varrho_0 + AT^2$.

The determined value of A equal to 0.5 $\mu\Omega$ cm K^{-2} suggests that the electron-spin-wave scattering is a dominant factor in the resistivity at low temperature.

For the Ce compound above the Néel temperature (near 30 K) a small minimum typical of the Kondo lattice in the temperature dependence resistivity is

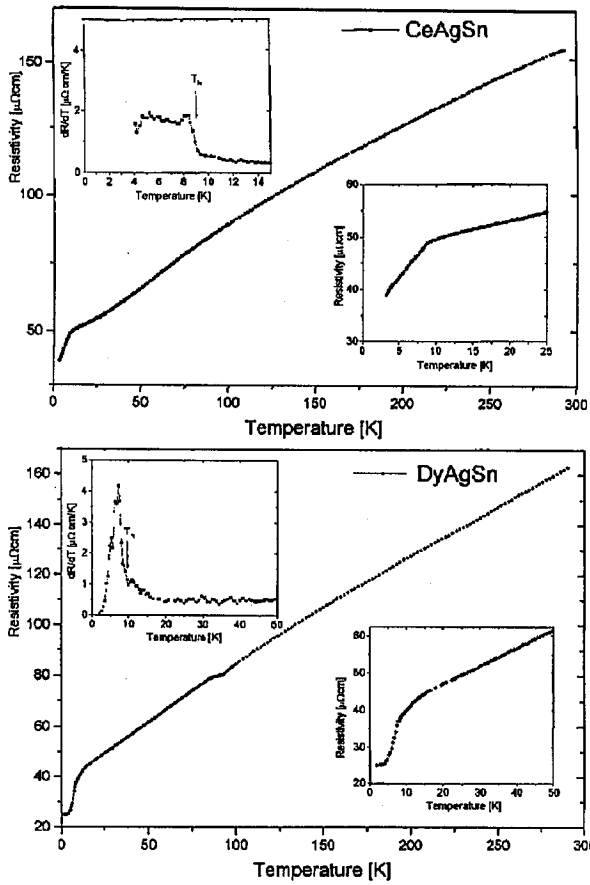

Fig. 9. Temperature dependences of the electrical resistivity: CeAgSn and DyAgSn. The inset shows the low temperature parts of $R(T)$ (lower parts) and differential resistivity $\mathrm{d}R/\mathrm{d}T$ (upper parts).

observed. The quasielastic neutron measurement [32] shows also the existence of the Kondo lattice behaviour below 40 K.

The temperature dependence of the resistivity above 50 K is fitted by the function $R(T) = R_0 + R_1 T + R_2 T^2 + R_3 T^3$. The determined values of R_0, R_1, R_2, and R_3 parameters are given in Table V. The obtained results show that at high temperatures linear and T^3 terms play a significant role which indicates the electron–phonon interaction in the presence of $s-d$ scattering [31].

The temperature dependence of electrical resistivity according to the Baber model [33] (which includes $s-d$ scattering) is given by the formula [34, 35]

$$R(T) = R_0 + B(T - \alpha T^3),$$

where

$$\alpha = \left\{ \frac{\pi^2}{6} k^2 \left[3 \left(\frac{1}{N} \frac{\mathrm{d}N}{\mathrm{d}E} \right)^2 - \frac{1}{N} \frac{\mathrm{d}^2 N}{\mathrm{d}E^2} \right]_{E_F} \right\}$$

TABLE V

Magnetic and electrical resistivity data for CeAgSn and DyAgSn.

Compound	Temperature region [K]	R_0 [$\mu\Omega$ cm]	R_1 [$\mu\Omega$ cm/K]	R_2 [$\mu\Omega$ cm/K^2]	$R_3 \times 10^{-6}$ [$\mu\Omega$ cm/K^2]
CeAgSn	10–300	45.3(2)	0.441(2)	0	−0.87(2)
	4–10	33.7(4)	1.72(1)	0	0
DyAgSn	10-300	37.46(6)	0.490(1)	0	−1.27(3)
	2–7.5	29.54(51)	0	0.205(20)	0

and N is the density state function, $\mathrm{d}N/\mathrm{d}E$ is its first and $\mathrm{d}^2N/\mathrm{d}E^2$ its second derivatives at the Fermi level. The determined values of α coefficient are 2.0×10^{-6} and 2.6×10^{-6} for CeAgSn and DyAgSn which indicates a small influence of the s–d scattering and it is in good agreement with the observed valence band structures. The $5d$ band of the rare earth atoms lies near the Fermi level.

7. Summary

The XPS measurements and calculations of electronic structure were performed for the RAgSn (R = Ce,Pr,Nd,Dy) series of compounds. They lead to the following conclusions:

1. The valence bands are determined mainly by the Ag $4d$ band. The calculated density of states (using the LMTO method) is comparable with the experimental one.
2. The XPS spectra of $3d_{5/2}$ and $3d_{3/2}$ of Ce, Pr, and Nd atoms have two peaks that correspond to the $3d^9_4f^n$ and $3d^94f^{n+1}$ configurations. The values of the spin–orbit splitting Δ_{SO} are equal to 18.8 eV for R = Ce, 20.2 eV for R = Pr and 22.6 eV for R = Nd.
3. The hybridization (coupling energy Δ) experimentally determined from the intensity ratio r based on the Gunnarsson–Schönhammer model are equal to 165 meV for R = Ce, 78 meV for R = Pr and 62 meV for R = Nd. It indicates that the hybridization energy decreases with an increase in the number of $4f$ electrons.
4. The total energy calculations performed for two models of crystal structure reported for these compounds [2, 3] show that the LiGaGe-type of structure is the stable one which is in agreement with the neutron diffraction data [3].

The temperature dependence of the electrical resistivity of CeAgSn and DyAgSn indicates an existence of anomalies at low temperatures connected with the magnetic phase transition. For CeAgSn an additional anomaly connected with the Kondo lattice effect is observed. At high temperatures, the resistivity is due to the s–d interaction. A fit of the temperature dependence of the CeAgSn and DyAgSn resistivity between 80 and 300 K, using a function $R(T) =$

$R_0 + B(T - \alpha T^3)$ implies that the α parameters are positive and small which is in agreement with the observed valence band structures.

Acknowledgments

One of us (A.J.) is greatly indebted to the Committee for Scientific Research for financial support (project No. 2 P03B 118 14). This work was partially supported by the Committee for Scientific Research (Poland) under the grant No. 2P03B 107 15.

References

[1] A. Szytuła, J. Leciejewicz, *Handbook of Crystal Structural and Magnetic Properties of Rare Earth Intermetallics*, CRC Press, Boca Raton 1994.

[2] D. Mazzone, D. Rossi, R. Marazza, R. Ferro, *J. Less-Common Met.* **80**, 47 (1981).

[3] S. Baran, J. Leciejewicz, N. Stüsser, A. Szytuła, A. Zygmunt, Yongfan Ding, *J. Magn. Magn. Mater.* **170**, 143 (1997).

[4] A. Adam, J. Sakurai, Y. Yamaguchi, H. Fujiwara, K. Mibu, T. Shinjo, *J. Magn. Magn. Mater.* **90-91**, 544 (1990).

[5] J. Sakurai, S. Nakatami, A. Adam, H. Fujiwara, *J. Magn. Magn. Mater.* **108**, 143 (1990).

[6] W. Bażela, J. Leciejewicz, K. Małetka, A. Szytuła, *J. Magn. Magn. Mater.* **117**, L1 (1992).

[7] W. Bażela, M. Guillot, J. Leciejewicz, K. Małetka, A. Szytuła, Z. Tomkowicz, *J. Magn. Magn. Mater.* **140-144**, 1137 (1995).

[8] O.K. Andersen, O. Jepsen, M. Sob, in: *Electronic Structure and its Applications*, Ed. M. Yussouff, Springer-Verlag, Berlin 1987, p. 2.

[9] D.A. Shirley, *Phys. Rev. B* **5**, 4709 (1972).

[10] U. von Barth, L. Hedin, *J. Phys. C* **5**, 391 (1972).

[11] D. Hu, D.C. Langreth, *Phys. Scr.* **32**, 391 (1985).

[12] M.S.S. Brooks, L. Nordsrom, B. Johansson, *J. Phys., Condens. Matter* **3**, 2357 (1991).

[13] J.J. Yeh, I. Lindau, *Atomic Data and Nuclear Data Tables* **32**, 1 (1985).

[14] J.K. Lang, Y. Baer, P.A. Cox, *J. Phys. F, Metal Phys.* **11**, 121 (1981).

[15] P.A. Cox, J.K. Lang, Y. Baer, *J. Phys. F, Met. Phys.* **11**, 113 (1981).

[16] S. Hüfner, *Photoemission Spectroscopy*, Springer Verlag, Berlin 1994, p. 453.

[17] H. Ogasawara, A. Kotani, B.T. Thole, *Phys. Rev. B* **50**, 12332 (1994).

[18] O. Gunnarsson, K. Schönhammer, *Phys. Rev. B* **28**, 4315 (1983).

[19] J.C. Fuggle, F.U. Hillebrecht, Z. Żołnierek, R. Lässer, Ch. Freiburg, O. Gunnarsson, K. Schönhammer, *Phys. Rev. B* **27**, 7330 (1983).

[20] A. Bianconi, T. Miyahara, A. Kotani, Y. Kitajima, T. Yokoyama, H. Kuroda, M. Funabashi, H. Arai, T. Okta, *Phys. Rev. B* **39**, 3380 (1989).

[21] H. Ogasawara, A. Kotani, B.T. Thole, *Phys. Rev. B* **44**, 5465 (1991).

[22] A. Ślebarski, A. Jezierski, A. Zygmunt, M. Neumann, S. Mähl, G. Borstel, *J. Magn. Magn. Mater.* **159,** 179 (1996).

[23] J.C. Fuggle, M. Campagna, Z. Żołnierek, R. Lässer, A. Platan, *Phys. Rev. Lett.* **45,** 1597 (1980).

[24] S. Doniach, M. Šunjić, *J. Phys. C* **3,** 285 (1970).

[25] A. Ślebarski, M. Neumann, S. Mähl, *Phys. Rev. B* **51,** 11113 (1995).

[26] R. Pöttgen, H. Borrmann, C. Felser, O. Jepsen, R. Henn, R.K. Kremer, A. Simon, *J. Alloys Comp.* **235,** 170 (1996).

[27] W. Schnelle, R. Pöttgen, R.K. Kremer, E. Gmelin, O. Jepsen, *J. Phys., Condens. Matter* **9,** 1435 (1997).

[28] M. Lenkewitz, S. Corsépius, G.R. Stewart, *J. Alloys Comp.* **241,** 121 (1996).

[29] A.R. Ball, D. Gignoux, D. Schmitt, F.Y. Zhang, *J. Magn. Magn. Mater.* **140-144,** 1121 (1995).

[30] E. Belorizky, J.J. Niez, P.M. Levy, *Phys. Rev. B* **23,** 3360 (1981).

[31] E. Gratz, M.J. Zuckerman, in: *Handbook on Physics and Chemistry of Rare Earths*, Eds. K.A. Gschneidner, L. Eyring, North-Holland, Amsterdam 1982, ch. 42, p. 117.

[32] D.T. Adroja, B.D. Rainford, A.J. Neville, *J. Phys., Condens. Matter* **9,** L391 (1997).

[33] W.G. Baber, *Proc. R. Soc. A* **158,** 130 (1933).

[34] H. Jones, *Handbook der Physik*, Vol. 19, Springer, Berlin 1956, p. 227.

[35] A. Kowalczyk, A. Jezierski, *J. Magn. Magn. Mater.* **188,** 361 (1998).